Supplementary Figures

Figure S1 (related to Figure 1 and 2). Expression of Vasa transgenes.

A) Schematic representation of transgenic constructs GFP-Vas^{WT}, GFP-Vas^{DQAD} and GFP-Vas^{GNT}

B) Expression patterns of *vas-Gal4* (top) and *matTub-Gal4* (bottom). Upper panels show schematic representation of the stages at which each driver is expressed. Bottom panels show confocal images of ovarioles expressing GFP-Vas^{WT} (GFP signal, green) under the control of each of the drivers. Scale bar indicates 50 μm.

C) Morphology of ovaries of wild-type (*w^{1118})* and *vas$^{D1/D1}$* flies. Scale bar indicates 500 μm.

D) Western blot analysis using antibodies against Vasa showing protein levels in ovaries of wild-type (*w^{1118}), vas$^{PD/D1}$*, *vas$^{PD/D1}$; vas-Gal4>GFP-Vas^{WT}*, *vas$^{PD/D1}$; vas-Gal4>GFP-Vas^{DQAD}*, *vas$^{PD/D1}$; vas-Gal4>GFP-Vas^{GNT}*, *vas$^{D1/D1}$*, *vas$^{D1/D1}$; vas-Gal4>GFP-Vas^{WT}*, *vas$^{D1/D1}$; vas-Gal4>GFP-Vas^{DQAD}* and *vas$^{D1/D1}$; vas-Gal4>GFP-Vas^{GNT}.* Tubulin served as a loading control.

E) Western blot analysis using antibodies against Vasa showing protein levels in early embryos produced by wild-type (*w^{1118}), vas$^{PD/D1}$*, *vas$^{PD/D1}$; vas-Gal4>GFP-Vas^{WT}*, *vas$^{PD/D1}$; vas-Gal4>GFP-Vas^{DQAD}*, *vas$^{PD/D1}$; vas-Gal4>GFP-Vas^{GNT} and vas$^{D1/D1}$; vas-Gal4>GFP-Vas^{WT}* flies. Tubulin served as a loading control.

Figure S2 (related to Figure 3). Localization of Aub and Ago3 in the egg-chamber.

A) Immunodetection of Aub and Vasa in stage 6-8 egg-chambers from wild-type (*w^{1118}), vas$^{PD/D1}$*, *vas$^{PD/D1}$; vas-Gal4>GFP-Vas^{WT}*, *vas$^{PD/D1}$; vas-Gal4>GFP-Vas^{DQAD}* and *vas$^{PD/D1}$; vas-Gal4>GFP-Vas^{GNT}* flies. Scale bars indicate 50 μm (egg-chamber) and 10 μm (nuage).

B) Immunodetection of Ago3 and Vasa in stage 6-8 egg-chambers from flies as in A. Scale bars indicate 50 μm (egg-chamber) and 10 μm (nuage).

C) Immunodetection of Aub and Vasa in stage 10 egg-chambers from wild-type (*w*^{1118}), *vas*$^{PD/D1}$, *vas*$^{PD/D1}$; *vas-Gal4>GFP-Vas*^{WT} and *vas*$^{PD/D1}$; *vas-Gal4>GFP-Vas*^{GNT} flies. Scale bars indicate 100 µm (egg-chamber) and 10 µm (posterior pole).

D) Immunodetection of Ago3 and Vasa in stage 10 egg-chambers from flies as in D. Scale bars indicate 100 µm (egg-chamber) and 10 µm (posterior pole).

Figure S3 (related to Figure 3). Localization of Aub and Ago3 in the egg-chamber and embryos.

A) Immunodetection of Aub and Vasa (upper panels) and Ago3 and Vasa (bottom panels) in stage 6-8 egg-chambers from *vas*$^{D1/D1}$; *vas-Gal4>GFP-Vas*^{WT} flies. Scale bars indicate 50 µm (egg-chamber) and 10 µm (nuage).

B) Immunodetection of Aub and Vasa (upper panels) and Ago3 and Vasa (bottom panels) in stage 10 egg-chambers from *vas*$^{D1/D1}$; *vas-Gal4>GFP-Vas*^{WT} flies. Scale bars indicate 100 µm (egg-chamber) and 10 µm (posterior pole).

C) Immunodetection of Aub and Vasa in early embryos (stage 1) produced by wild-type (*w*^{1118}), *vas*$^{PD/D1}$, *vas*$^{PD/D1}$; *vas-Gal4>GFP-Vas*^{WT}, *vas*$^{PD/D1}$; *vas-Gal4>GFP-Vas*^{GNT} *and vas*$^{D1/D1}$; *vas-Gal4>GFP-Vas*^{WT} flies. Scale bars indicate 100 µm (embryo) and 20 µm (posterior pole).

D) Immunodetection of Ago3 and Vasa in early embryos (stage 1) produced by flies as in C. Scale bars indicate 100 µm (embryo) and 20 µm (posterior pole).

Figure S4 (related to Figure 4). GFP-Vasa co-immunoprecipitation analyses.

A) Correlation analysis of two replicates of GFP-Vas^{WT} and GFP-Vas^{DQAD} co-IPs (co-IP1, left chart; co-IP2, right chart). Correlation was determined using Pearson's correlation coefficient calculation.

B) Venn diagrams comparing two biological replicates (co-IP1, blue circle; co-IP2, red circle) of GFP-Vas^{WT} (left) and GFP-Vas^{DQAD} (right) co-IPs.

C) Venn diagram of enriched (>2 fold) proteins represented in Figure 3C from two biological

replicates of GFP-Vas^{WT} and GFP-Vas^{DQAD} co-IPs.

D) Gene Ontology enrichment analysis of biological processes for genes enriched in GFP-Vas^{WT} and GFP-Vas^{DQAD} co-IPs.

E) Gene Ontology enrichment analysis of cellular component for genes enriched in GFP-Vas^{WT} and GFP-Vas^{DQAD} co-IPs.

Figure S5 (related to Figure 5). Age-dependent progression of ovarian atrophy.

A) Images of ovaries from 3-day, 10-day, and 20-day old wild-type (*w*^{1118}*)*, *vas*$^{D1/D1}$, *vas*$^{D1/D1}$*; vas-Gal4>GFP-Vas*^{WT} and *vas*$^{D1/D1}$*; matTub-Gal4>GFP-Vas*^{WT} flies. Scale bar indicates 500 µm.

B) Confocal images of ovarioles from 3-day, 10-day, and 20-day old wild-type (*w*^{1118}*)*, *vas*$^{D1/D1}$, *vas*$^{D1/D1}$*; vas-Gal4>GFP-Vas*^{WT} and *vas*$^{D1/D1}$*; matTub-Gal4>GFP-Vas*^{WT} flies. Pyknotic egg-chambers are marked with asterisk. Scale bar indicates 100 µm.

Figure S6 (related to Figure 6). Control of *mnk* RNAi efficiency.

A) Q-PCR analysis of *mnk* mRNA in ovaries from wild-type (*w*^{1118}*)*, *vas*$^{D1/D1}$, *vas*$^{D1/D1}$*; vas-Gal4>TRiPmnk*, *vas*$^{D1/D1}$*; matTub-Gal4>TRiPmnk* and *vas*$^{D1/D1}$*; vas-Gal4>TRiPw* flies. Expression level of *mnk* in *w*^{1118} was set to 1 and normalized to *rp49* mRNA in individual experiments. Error bars represent the standard deviation among three biological replicates.

B) Images of ovaries (left) and *in situ* detection of *mnk* mRNA by FISH (right), in wild-type (*w*^{1118}*)*, *vas*$^{D1/D1}$, *vas*$^{D1/D1}$*; vas-Gal4>TRiPmnk*, *vas*$^{D1/D1}$*; matTub-Gal4>TRiPmnk* and *vas*$^{D1/D1}$*; vas-Gal4>TRiPw* ovaries. Scale bars indicate 500 µm (ovaries) and 100 µm (ovarioles).

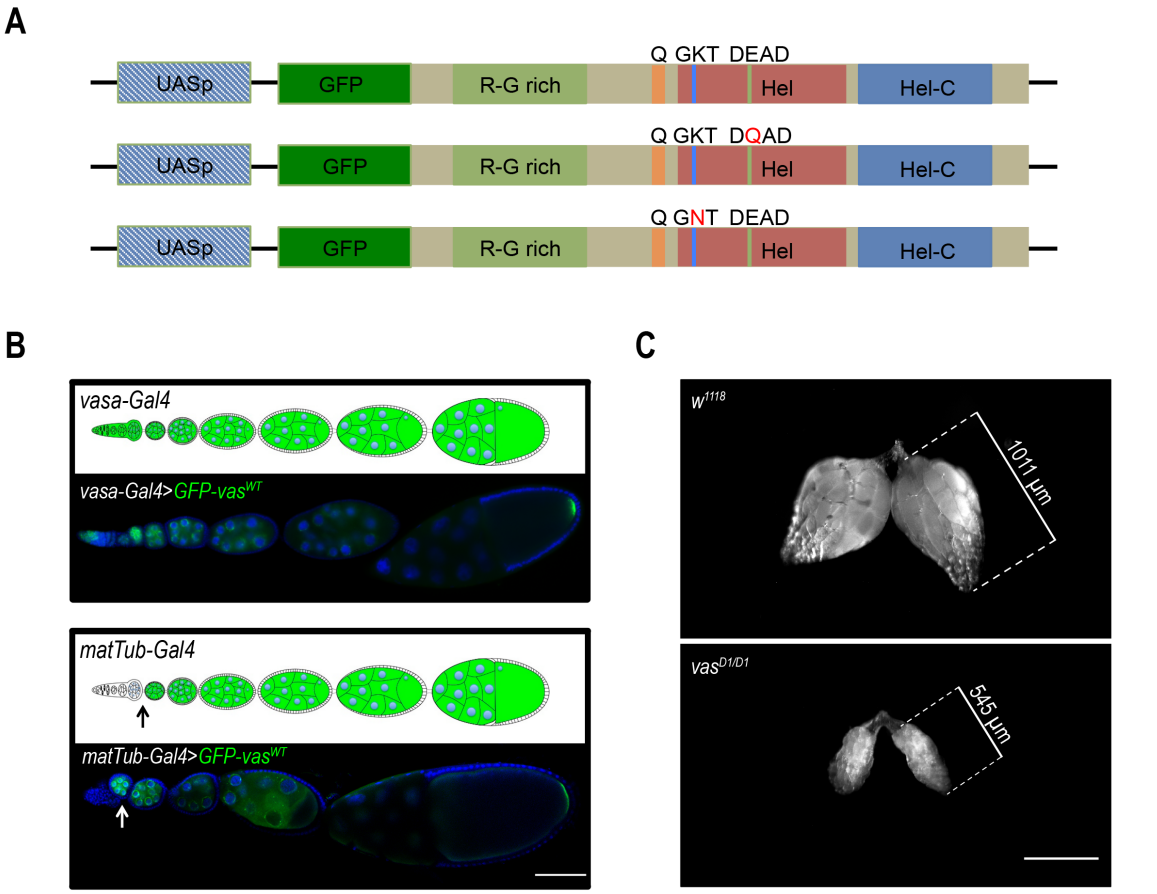

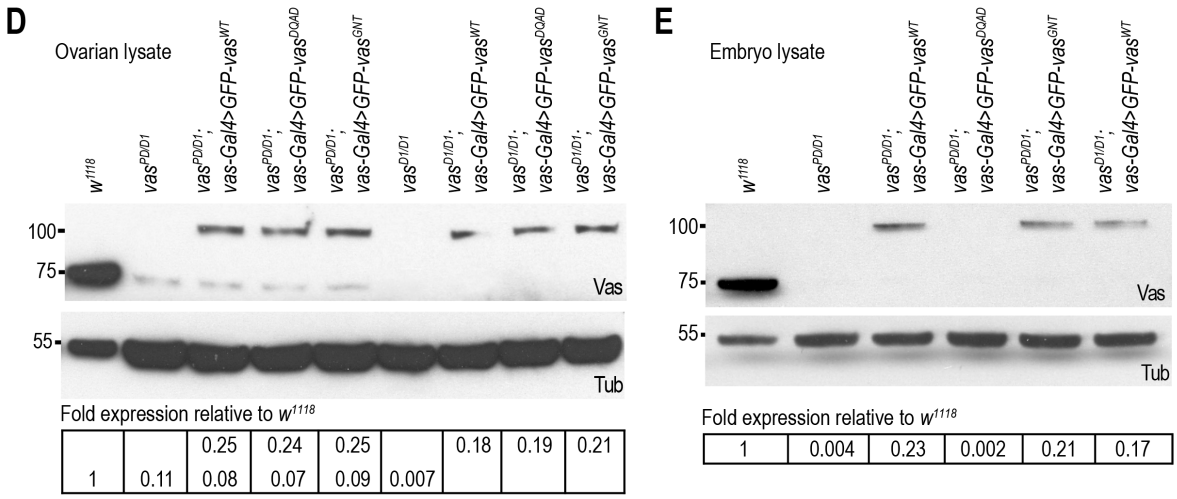

Fold expression relative to w^{1118}

1	0.11	0.25 0.08	0.24 0.07	0.25 0.09	0.007	0.18	0.19	0.21

Fold expression relative to w^{1118}

1	0.004	0.23	0.002	0.21	0.17

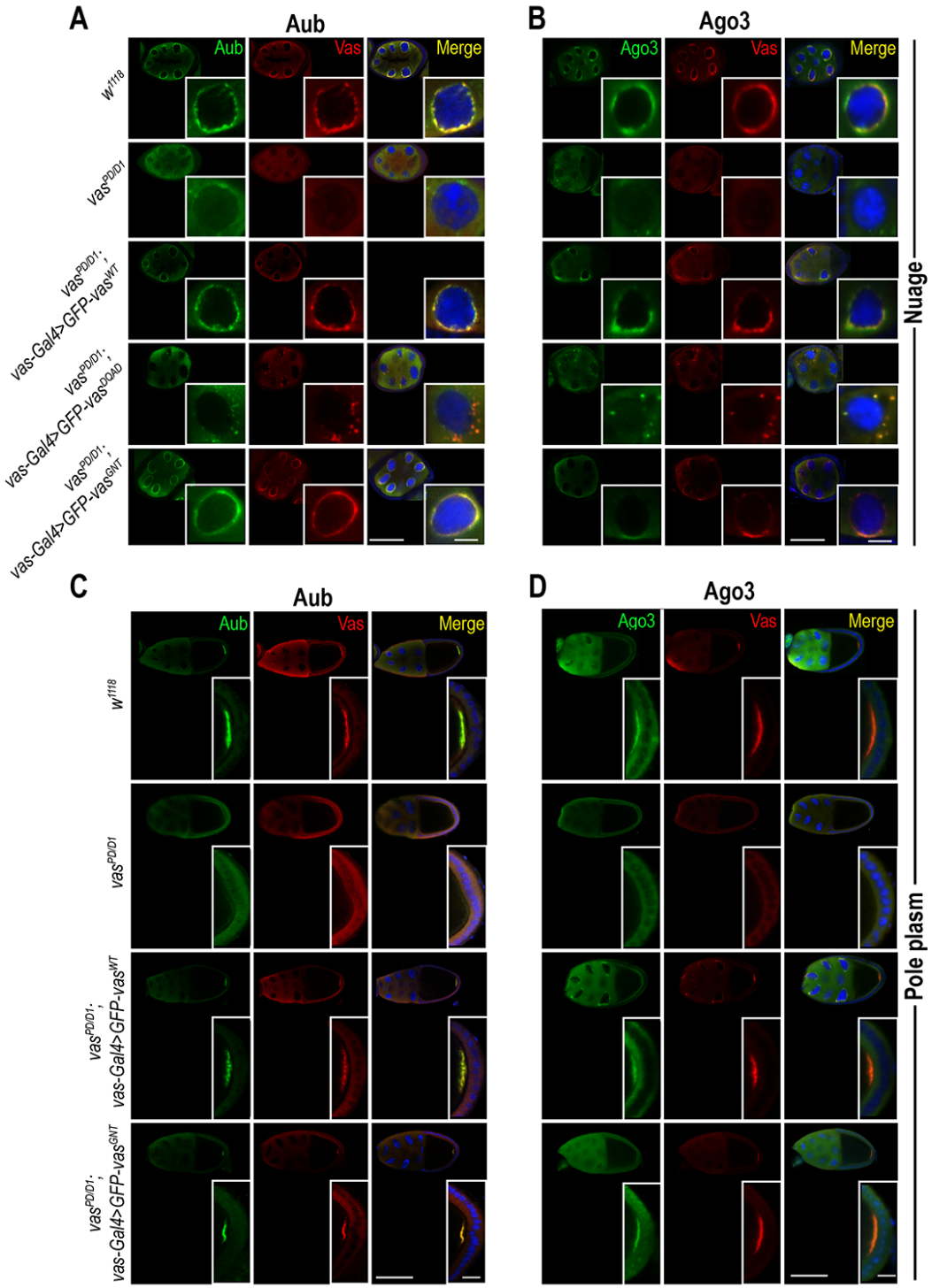
A
Aub
Aub
Vas
Merge
w1118
VasPD/D1
VasPD/D1; vas-Gal4>GFP-vasWT
VasPD/D1; vas-Gal4>GFP-vasDQAD
VasPD/D1; vas-Gal4>GFP-vasGNT
B
Ago3
Ago3
Vas
Merge
Nuage
C
Aub
Aub
Vas
Merge
w1118
VasPD/D1
VasPD/D1; vas-Gal4>GFP-vasWT
VasPD/D1; vas-Gal4>GFP-vasGNT
D
Ago3
Ago3
Vas
Merge
Pole plasm

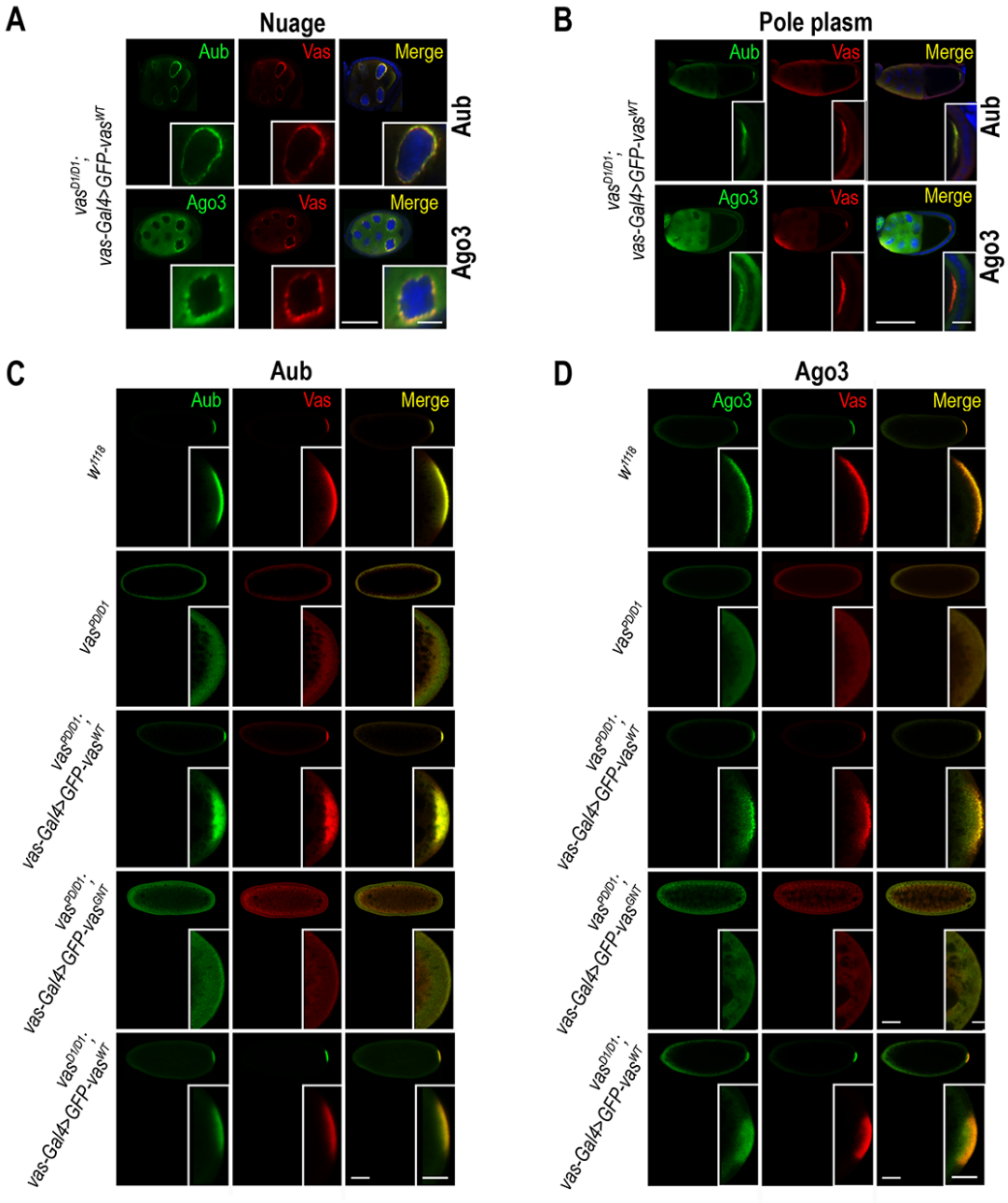
A
Nuage
Aub
Vas
Merge
Ago3
vasD1/D1; vas-Gal4>GFP-vasWT
B
Pole plasm
C
Aub
W1118
vasPD/D1
vasPD/D1; vas-Gal4>GFP-vasWT
vasPD/D1; vas-Gal4>GFP-vasGNT
vasD1/D1; vas-Gal4>GFP-vasWT
D
Ago3

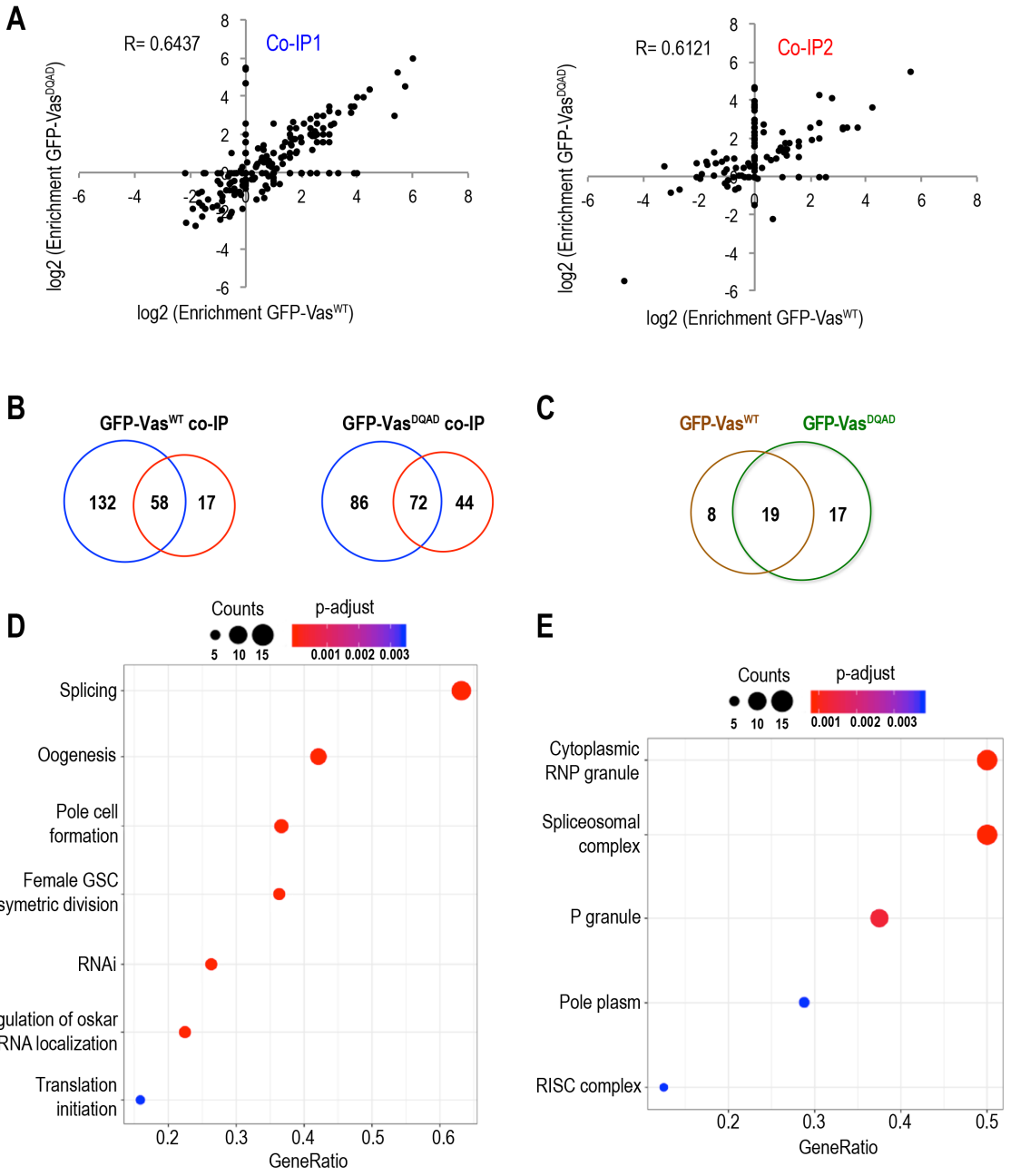
A
R= 0.6437
Co-IP1
log2 (Enrichment GFP-Vas^DQAD)
log2 (Enrichment GFP-Vas^WT)
R= 0.6121
Co-IP2
log2 (Enrichment GFP-Vas^DQAD)
log2 (Enrichment GFP-Vas^WT)
B
GFP-Vas^WT co-IP
132
58
17
GFP-Vas^DQAD co-IP
86
72
44
C
GFP-Vas^WT
GFP-Vas^DQAD
8
19
17
D
Counts
5 10 15
p-adjust
0.001 0.002 0.003
Splicing
Oogenesis
Pole cell formation
Female GSC assymetric division
RNAi
Regulation of oskar mRNA localization
Translation initiation
0.2 0.3 0.4 0.5 0.6
GeneRatio
E
Counts
5 10 15
p-adjust
0.001 0.002 0.003
Cytoplasmic RNP granule
Spliceosomal complex
P granule
Pole plasm
RISC complex
0.2 0.3 0.4 0.5
GeneRatio

Durdevic et al. Suppl. Fig5

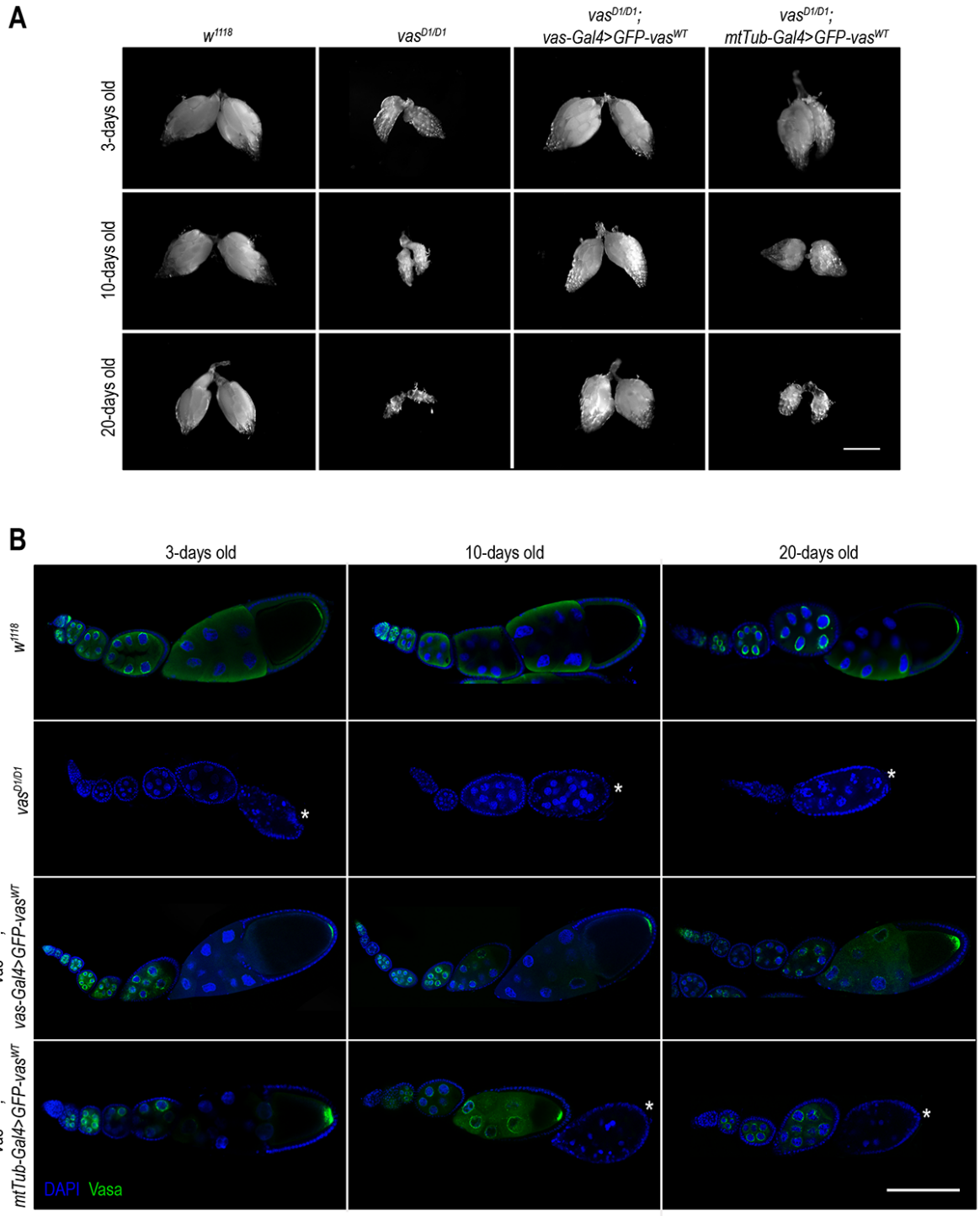

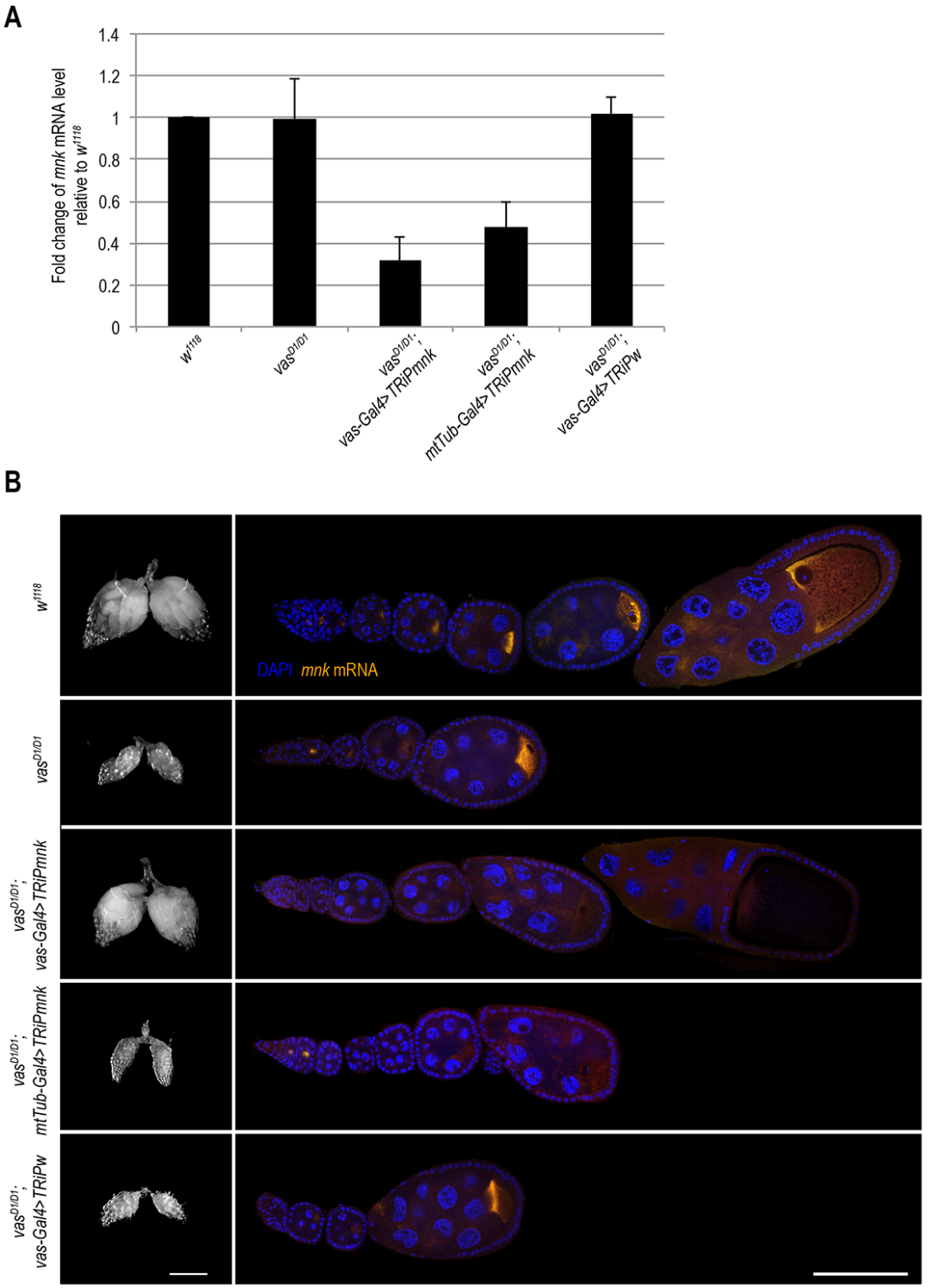
A
Fold change of mnk mRNA level relative to w1118
1.4
1.2
1
0.8
0.6
0.4
0.2
0
w1118
vasD1/D1
vasD1/D1; vas-Gal4>TRiPmnk
vasD1/D1; mtTub-Gal4>TRiPmnk
vasD1/D1; vas-Gal4>TRiPw
B
w1118
vasD1/D1
vasD1/D1; vas-Gal4>TRiPmnk
vasD1/D1; mtTub-Gal4>TRiPmnk
vasD1/D1; vas-Gal4>TRiPw
DAPI mnk mRNA